photonics

MDPI

Article

Measurements of Carrier Concentration, Mobility and Crystalline Properties Along the Growth Direction in MOCVD-Grown GaN-on-Sapphire by Cross-Section Raman Spectroscopy

Guang Chen [1,2], Manika Tun Nafisa [3], Yun-Chen Chung [4], Subiao Bian [1], Zhe Chuan Feng [2,5,*], Hsiang-Lin Liu [4], Kang Yang [6], Jixiong Li [6], Jeffrey Yiin [3], Gu Xu [7,8], Weijie Lu [9], Benjamin Klein [3], Ian Ferguson [3] and Changcai Cui [1,*]

1 College of Metrology Measurement and Instrument, China Jiliang University, Hangzhou 310018, China; b24020804001@cjlu.edu.cn (G.C.); biansubiao@cjlu.edu.cn (S.B.)
2 College of Mechanical Engineering, Jiamusi University, Jiamusi 154007, China
3 Southern Polytechnic College of Engineering and Engineering Technology, Kennesaw State University, Marietta, GA 30060, USA; mnafisa@students.kennesaw.edu (M.T.N.); jyiin@kennesaw.edu (J.Y.); bklein8@kennesaw.edu (B.K.); ifergus3@kennesaw.edu (I.F.)
4 Department of Physics, National Taiwan Normal University, Taipei 11677, Taiwan; coldlizem@gmail.com (Y.-C.C.); hliu@ntnu.edu.tw (H.-L.L.)
5 Science Exploring Lab, Arbour Glenn Drive, Lawrenceville, GA 30043, USA
6 Wuhan Eoptics Technology Co., Ltd., Wuhan 430075, China; kang.yang@eoptics.com.cn (K.Y.); jixiong.li@eoptics.com.cn (J.L.)
7 Shenzhen Institute for Advanced Study, University of Electronic Science and Technology of China, Longhua District, Shenzhen 518110, China; xugu@mcmaster.ca
8 Department of Materials Science and Engineering, McMaster University, Hamilton, ON L8S 4L8, Canada
9 Hexagonal Scientific Lab, LLC., Dayton, OH 45459, USA; wlu@hsl-mat.com
* Correspondence: zfeng6@kennesaw.edu or zcfeng@ntu.edu.tw (Z.C.F.); cuichc@cjlu.edu.cn (C.C.); Tel.: +1-(470)-967-6465 (Z.C.F.); +86-186-9568-2866 (C.C.)

Abstract

GaN-on-sapphire structure is currently playing an important role in developing modern optoelectronic and electronic devices. Cross-sectional Raman scattering (RS) measurements were conducted along the growth direction of GaN-on-sapphire structures; the 4.0 μm R4 and 7.6 μm N7 layers were measured using step intervals of 0.5 μm and 1.0 μm, respectively. Characterization techniques, such as scanning electron microscopy, optical transmission and spectroscopic ellipsometry, have been applied to these GaN/sapphire structures and provide information on the crystalline properties of the two GaN films. Cross-sectional Raman measurements showed sample-dependent shifts in the fitted GaN E_2(high) and E_1(LO) peak positions. The fitted E_2(high) peak positions were used to estimate the relative stress profiles, while spatial correlation model analysis provided model-dependent estimates of the effective phonon correlation lengths and damping constants. Longitudinal optical phonon–plasmon coupling fitting of the E_1(LO) modes was used to estimate the carrier concentration and mobility. The distinctive findings may enhance the comprehension of GaN/sapphire and present valuable benchmarks for others within this field.

Keywords: gallium nitride (GaN); MOCVD; cross-section Raman scattering; carrier concentration and mobility; phonon-plasmon coupling; SEM

Check for updates

Received: 22 June 2026
Revised: 3 September 2026
Accepted: 17 September 2026
Published: 19 September 2026

Copyright: © 2026 by the authors. Licensee MDPI, Basel, Switzerland. This article is an open access article distributed under the terms and conditions of the Creative Commons Attribution (CC BY) license.

1. Introduction

Gallium Nitride (GaN) growth on sapphire has been studied since the late 1960s, beginning with Melton and Pankove [1]. Nakamura et al. demonstrated blue laser diodes based on a GaN-on-sapphire structure [2]. Amano presented a Nobel Lecture with an overview of historical breakthroughs for successful MOVPE of GaN on sapphire and p-type doping [3]. Gao et al. reviewed recent advances in III-nitride flexible optoelectronics, from materials to applications [4]. GaN/sapphire structures have been used in a wide range of electronic and optoelectronic devices [5]. Recent MOCVD studies have demonstrated high-efficiency InGaN-based green LEDs and high-power AlGaN-based deep-UV LEDs on sapphire-related structures [6,7]. Raman scattering is an established non-destructive method for characterizing GaN and related materials [8]. Previous studies have examined cross-sectional Raman spectra [9], structural and optical properties [10], and anisotropic strain using polarized Raman spectroscopy [11]. Nootz et al. [12] correlated spatially resolved Raman shifts with dislocation density, whereas Chaldyshev et al. [13] investigated laterally epitaxially overgrown GaN/sapphire. Duan et al. [14] combined Raman spectroscopy with HRXRD to characterize GaN grown on sapphire and 4H-SiC, while Belyaev et al. [15] used confocal Raman microscopy to profile strain and carrier concentration in a cleaved GaN Gunn-diode structure. Additional optical properties of GaN-based structures have also been reported [16]. These studies demonstrate that Raman-based stress and carrier analyses are established methods, while the sample structures, measurement configurations, and complementary characterization methods differ from those used in the present work. Recent GaN/sapphire studies have also addressed photonic and power devices, leakage mechanisms, acoustic structures, sensors, carrier transport, and temperature-dependent optical properties [17–24].

In this work, cross-sectional Raman spectroscopy is used to compare two MOCVD-grown GaN/sapphire samples with GaN layer thicknesses of 7.6 and 4.0 μm. SEM, OT, and SE were used to provide complementary structural and optical information. First, two GaN-on-sapphire samples with various GaN film thicknesses were characterized by cross-section scanning electron microscopy (SEM), optical transmission (OT) and spectroscopic ellipsometry (SE), providing complementary structural and optical characterization. Second, cross-section Raman scattering revealed the GaN E_2(high) and E_1(LO) band shift, indicating the variation of the compressive stress along the film growth direction. The results from this investigation could expand the understanding of the investigated GaN/sapphire structures and provide useful references for this field.

2. GaN-on-Sapphire Samples

GaN films were grown on c-sapphire by metal-organic chemical vapor deposition (MOCVD) under low-pressure conditions (10-250 Torr), with trimethylgallium (TMGa, $Ga(CH_3)_3$) and ammonia (NH_3) as gallium and nitrogen sources, respectively, plus with hydrogen (H_2) acting as the carrier gas. The growth process began with the formation of ~200 Å GaN buffer layer at ~530 °C, followed by increasing the substrate temperature to ~1040 °C for the deposition of the main GaN layer [10]. Low-temperature GaN nucleation layers grown on sapphire are known to exhibit growth- and annealing-dependent changes in surface morphology, crystalline phase, and optical properties [25]. Related MOVPE studies of GaN heteroepitaxy have also shown that AlGaN interlayers can modify the strain state, while SiN masking can contribute to threading-dislocation reduction during subsequent GaN growth [26]. Two GaN-on-sapphire samples, N7 and R4, with their original run numbers of n7600 and r4056, respectively, are studied in this work. GaN film thicknesses were determined to be 7.6 μm for N7 and 4.0 μm for R4 from cross-sectional imaging using a field-emission scanning electron microscope (JEOL JSM-7000F,

Center for Condensed Matter Sciences, National Taiwan University, Taipei, Taiwan and the manufacturer JEOL was located in Akishima, Tokyo, Japan.) (FESEM, Sigma500/VP, ZEISS), as shown in Figure 1. N7 and R4 were selected as representative GaN/sapphire samples with different GaN layer thicknesses and well-defined cross-sections suitable for Raman line scanning.

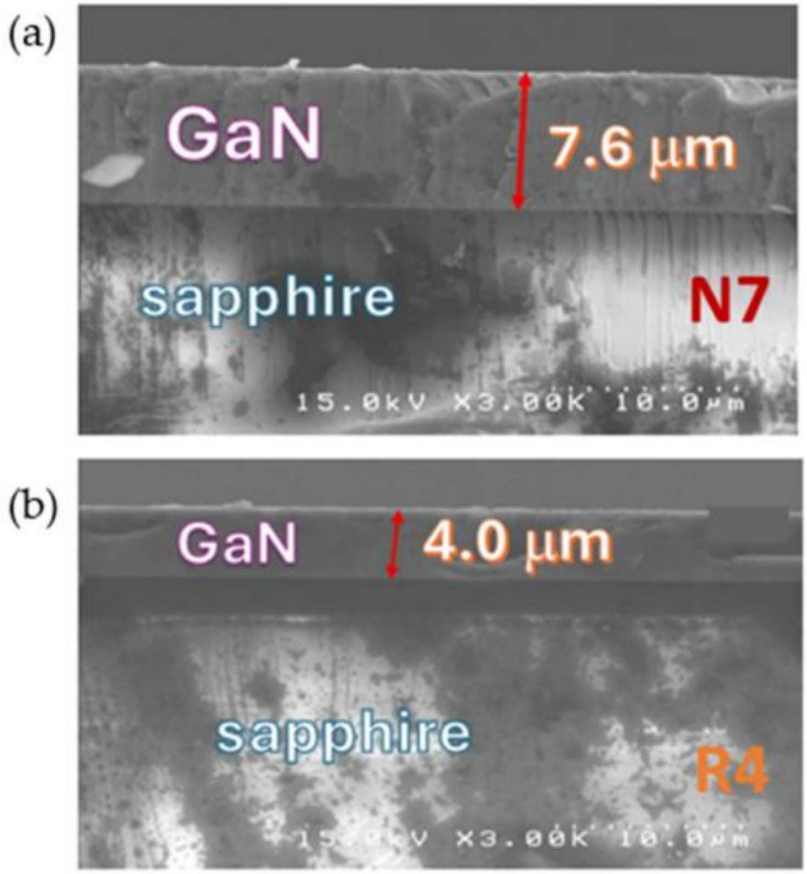


Figure 1. Cross-section scanning electron microscopy (SEM) patterns for two GaN-on-sapphire samples of (**a**) N7 with *d* (GaN) = 7.6 μm and (**b**) R4 with *d* (GaN) = 4.0 μm, respectively.

GaN growth on sapphire generally evolves from a low-temperature nucleation or buffer layer through an initial three-dimensional growth and coalescence stage to a smoother two-dimensional high-temperature GaN layer [1,3,25]. These growth stages may differ in strain relaxation, defect evolution, and impurity incorporation. Because the individual regions were not independently identified in the present samples, this growth sequence is used only as a qualitative framework for interpreting the depth-dependent results rather than for assigning discrete layer boundaries.

For the present samples, OT records the integrated optical response of the complete GaN/sapphire structure and may include contributions from the thin buffer and interfacial regions. SE mainly provides model-derived thickness, surface roughness, and optical constants for the dominant GaN layer. Cross-sectional Raman spectroscopy probes micrometer-scale variations within the main GaN layer, but the present sampling intervals are insufficient to isolate the approximately 200 Å buffer layer or to identify a sharp boundary between the three-dimensional and two-dimensional growth regions. Measurements near and beyond the nominal GaN/sapphire interface were retained for completeness. Because these spectra may contain contributions from both GaN and sapphire owing to spatial averaging, no layer-specific stress interpretation is assigned to these points.

3. Analysis and Discussion of Measurement Results

3.1. OT Measurements

Room-temperature (RT) UV–visible OT spectra of GaN-on-sapphire samples were measured by a UV–visible spectrophotometer (OmniAs, Zolix). The instrument provided a spectral resolution of 0.1 nm and an accuracy of approximately 0.3%. Figure 2a shows the OT spectra of N7 and R4 over 3000–29,000 cm^{-1}, corresponding to wavelengths of 345–3300 nm and photon energies of 0.38–3.59 eV. The periodic oscillations in the figure are due to multiple reflections between the air–GaN and GaN–substrate interfaces [27].

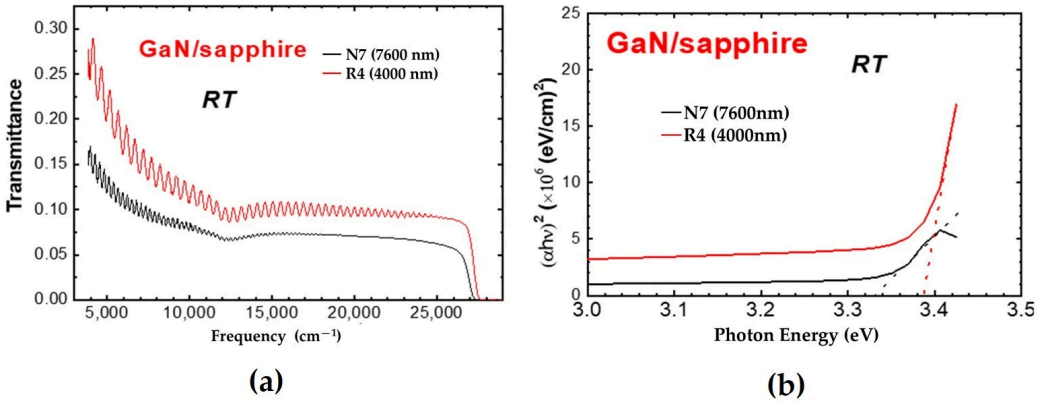


Figure 2. (**a**) OT spectra in frequency range of 3000–29,000 (cm^{-1}) and (**b**) relations of $(\alpha h\nu)^2$ versus photon energy (eV) in energy range of 3.0–3.5 eV of two GaN-on-sapphire samples of N7 and R4, respectively.

For the present comparative analysis, the apparent absorption coefficient (α) was estimated from the measured transmittance (T) using the following simplified Beer–Lambert-type relation:

$$\alpha t = \ln(1/T) \quad (1)$$

where t is the GaN layer thickness obtained from the cross-sectional SEM measurements shown in Figure 1. Because this simplified relation does not explicitly correct for reflection losses or thin-film interference, α is treated as an apparent absorption coefficient for comparative analysis. Further, the relationship between the absorption coefficient (α) and photon energy ($h\nu$ in eV) can be described by the Tauc empirical relation [27,28]

$$\alpha h\nu = C\left(h\nu - E_g\right)^{1/2} \quad (2)$$

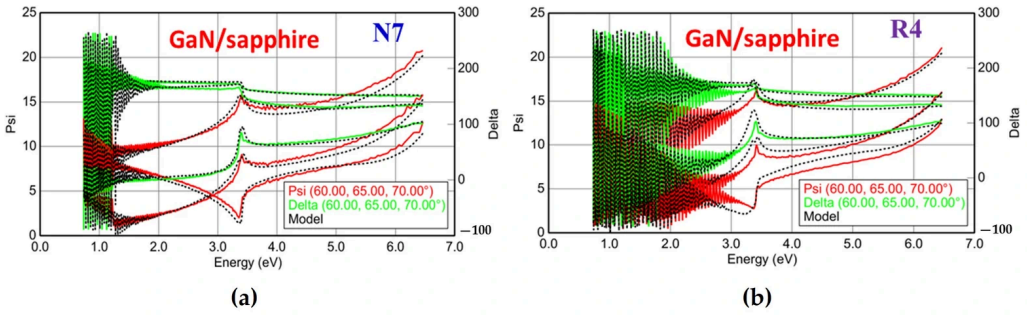
where C is a constant. Figure 2b shows the corresponding relations of $(\alpha h\nu)^2$ versus photon energy (eV) for the two GaN films, from which, through extrapolating the linear part of the $(\alpha h\nu)^2$~eV curve to reach the X-axis, the band gap energy E_g (GaN) can be obtained, i.e., using the Tauc method [28]. Figure 2b shows the E_g (GaN) values to be 3.34 eV for N7 and 3.39 eV for R4. Both values are slightly less than the stress-free E_g (GaN) value of ~3.42 eV [2,4].

Optical transmission records the through-thickness optical response of the complete GaN/sapphire structure and therefore complements the model-based SE analysis. The observed differences may contain contributions from the GaN layer, buffer region, and interfaces. However, no layer-specific assignment is made from the present OT measurements.

3.2. Spectroscopic Ellipsometry (SE) Measurements

A dual-rotation compensation Mueller matrix ellipsometer (ME-L model, Wuhan Eoptics Technology Co., Ltd., Wuhan, China) was used at room temperature to measure

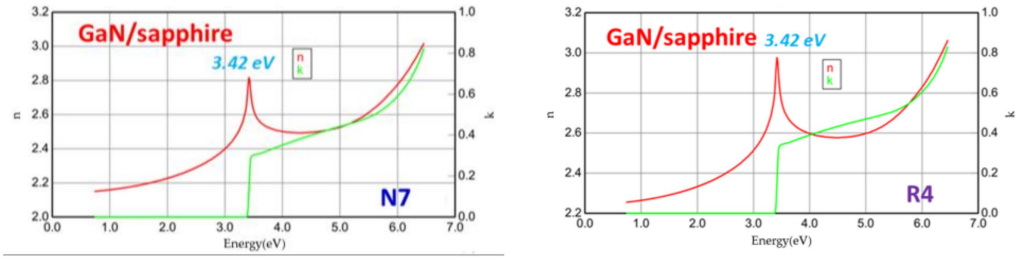
SE spectra at three incidence angles of 60°, 65°, and 70°. The spectra were fitted using CompleteEASE software (Version: 5.29) (J. A. Woollam Co., USA), and the fitted quantities included the GaN thickness, surface roughness, and optical constants. Figure 3 displays the typical RT spectroscopic ellipsometry (SE) spectra measured at incidence angles of 60°, 65°, and 70° and in the energy range of 0.75–6.4 eV of GaN-on-sapphire samples for (a) N7 and (b) R4, respectively. Fitting with CompleteEASE yielded GaN film thicknesses of 7.90 μm for N7 and 4.28 μm for R4, together with surface roughness values of 21 nm and 35 nm, respectively. The SE-determined GaN film thicknesses are approximately 4% and 7% higher than those determined from the cross-sectional SEM measurements for N7 and R4, respectively. These slight differences may have arisen from different measurements at different spots of the samples.



(a) **(b)**

Figure 3. RT spectroscopic ellipsometry (SE) spectra with incident angles of 60°, 65° and 70°, in the energy range of 0.75–6.4 eV of GaN-on-sapphire samples for (**a**) N7 and (**b**) R4, respectively.

The optical parameters of refractive index n, extinction coefficient k and optical absorption α, as well as their dependence on energy (eV), can be deduced from measured SE spectra. Figure 4 presents the RT SE spectral-deduced relationships of n~eV and k~eV in 1.0–6.5 eV for GaN-on-sapphire samples of (a) N7 and (b) R4, respectively. They show the n~eV curves with maxima peaks at about 3.42 eV and the k~eV curves having the change near the absorption edge with the midpoints near 3.42 eV also, and both are close to the E_g (GaN).



(**a**) (**b**)

Figure 4. RT SE spectra-deduced relationships of refractive index n vs. eV (red) and extinction coefficient k vs. eV (green) in the energy range of 0.75–6.45 eV of GaN-on-sapphire samples for (**a**) N7 and (**b**) R4, respectively.

Figure 5 shows the RT SE spectral-deduced relationships of α~eV in 3.0–4.0 eV for GaN/sapphire samples of (a) N7 and (b) R4, respectively. They show the α~eV curves having sharp absorption edge between 3.40–3.45 eV, like the k~eV curves in Figure 4, due to $\alpha = 4\pi k/\lambda$.

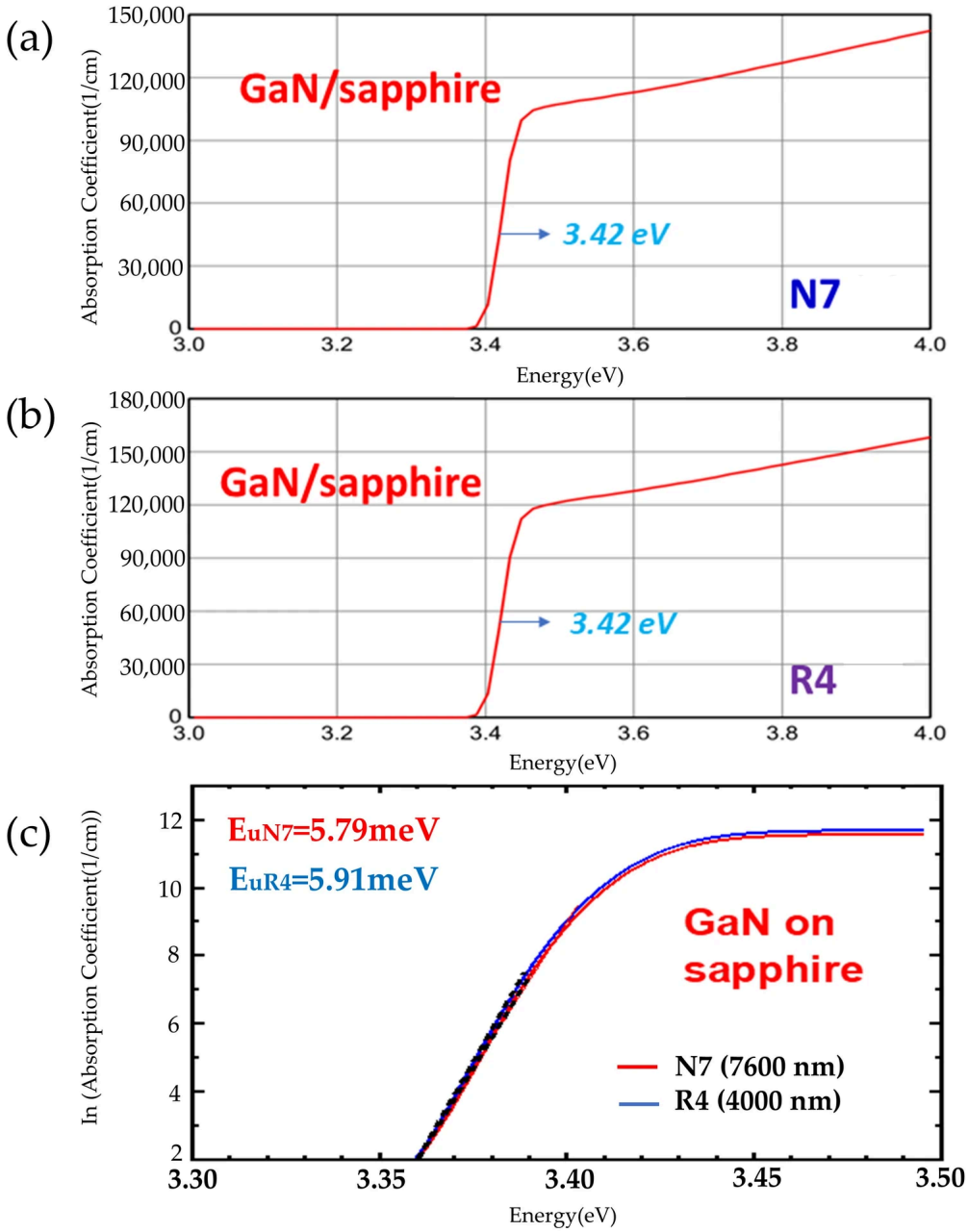


Figure 5. RT SE-deduced relationships of absorption coefficient α~eV in 3.0–4.0 eV of GaN-on-sapphire (**a**) N7 and (**b**) R4, respectively. (**c**) Deduced ln(α)~eV in 3.30–3.50 eV of GaN/sapphire N7 and R4.

Below approximately 3.405 eV, the absorption-coefficient spectra exhibit exponential tails attributed to structural disorder and electron–phonon interactions. These Urbach tails are described by Equation (3) [29].

$$1/E_U = \mathrm{d}(\ln(\alpha))/\mathrm{d}(h\nu) \quad (3)$$

where the Urbach energy E_U is acquired from the inverse slope of the derivative of ln(α) with respect to photon energy $h\nu$(eV). Because the detailed dielectric-function parameterization, surface-layer model, and near-band-edge fitting residuals are not available for the present analysis, the SE-derived absorption coefficient and Urbach energy are treated as model-dependent quantities. The reported Urbach energies are therefore used only for comparison between N7 and R4.

Figure 5c exhibits the SE-deduced ln(α) versus photon energy relationships for N7 and R4. The apparent Urbach energies obtained from the linear region are 5.79 meV for N7 and 5.91 meV for R4. These values are lower than the value of approximately 18 meV reported for GaN/Si [29].

Piccardo et al. reported the Urbach tails in semiconductors being commonly linked to disorder in composition and noted the GaN's E_U of about 12–15 meV [30]. S. Chichibu et al. obtained the temperature-dependent Urbach energy in a wurtzite GaN epilayer, which varied from 12 meV at 300 K down to 6.3 meV at 80 K [31]. Finn et al. reported Urbach energies in the range of 11–13 meV for $Al_{0.48}Ga_{0.52}N/Al_{0.63}Ga_{0.37}N$ structures [32]. Ugur et al. reviewed Life on the Urbach Edge and listed more E_U values of semiconductors, PV materials and Perovskites, with E_U = 7.5 meV for GaAs and 9.4 meV for InP, and all others beyond 10 meV [33]. Ledinsky et al. reported that methylammonium lead iodide ($CH_3NH_3PbI_3$) exhibits lower Urbach energy in comparison with conventional crystalline semiconductors, such as Si, GaAs, InP and GaN [34].

3.3. Cross-Section Raman Measurements and Stress Distribution

Cross-sectional micro-Raman measurements were performed at room temperature in a backscattering configuration using a 532 nm diode laser and a SENTERRA spectrometer. The instrument incorporates the Sure_Cal automatic continuous-calibration system, which records the laser excitation line and neon-lamp emission lines with each spectrum to correct changes in the laser and spectrograph. The manufacturer-specified wavenumber accuracy and precision of the calibrated Raman-shift axis are better than 0.1 cm^{-1}. Each sample was mounted vertically in the narrow slot of a clamp and scanned from the GaN surface toward the sapphire substrate, with nominal sampling intervals of 1.0 μm for N7 and 0.5 μm for R4. These intervals represent the spacing between adjacent measurement positions rather than the effective spatial resolution. Spectra were examined over 500–770 cm^{-1}. The E_2(high) peaks were fitted with a Gaussian function over 564–572 cm^{-1} for N7 and 567–572 cm^{-1} for R4, while the E_1(LO) regions analyzed were 730–750 cm^{-1} for N7 and 736–752 cm^{-1} for R4. The specified wavenumber accuracy is distinct from the spectral resolution, which depends on the optical configuration. Since the archived records do not provide the complete optical and acquisition settings—including the grating, slit or pinhole, objective, laser power at the sample, acquisition time, accumulation number, and repeated-scan information—the configuration-specific spectral and effective spatial resolutions and experimental error bars cannot be reliably determined for this dataset. Peak positions are therefore presented as fitted values, and spectra near the nominal GaN/sapphire interface are interpreted cautiously because the finite probe volume may sample both materials.

The fitted E_2(high) peak positions were used to estimate relative stress trends along the GaN growth direction. The spatial correlation model (SCM) was applied to obtain effective phonon correlation lengths and damping parameters, while longitudinal optical phonon–plasmon coupling (LOPC) fits to the E_1(LO) mode were used to estimate carrier concentration and mobility. These quantities are treated as model-dependent parameters for comparing N7 and R4 rather than as independently calibrated measurements.

Figure 6a,b present Raman spectra (ex. 532 nm, RT) in a standard backscattering geometry for GaN/sapphire N7 and R4, with dominant contributions from sapphire substrate, marked with *, displaying four peaks in 370–450 cm^{-1}, plus peaks near 578 cm^{-1} and 754 cm^{-1} [9]. The GaN E_2(high) phonon at ~568 cm^{-1} in sample N7 is much stronger than the thinner samples in R4. Additionally, GaN A_1(LO) mode is detected at the lower-frequency wing of the sapphire-related peak near 754 cm^{-1} [9].

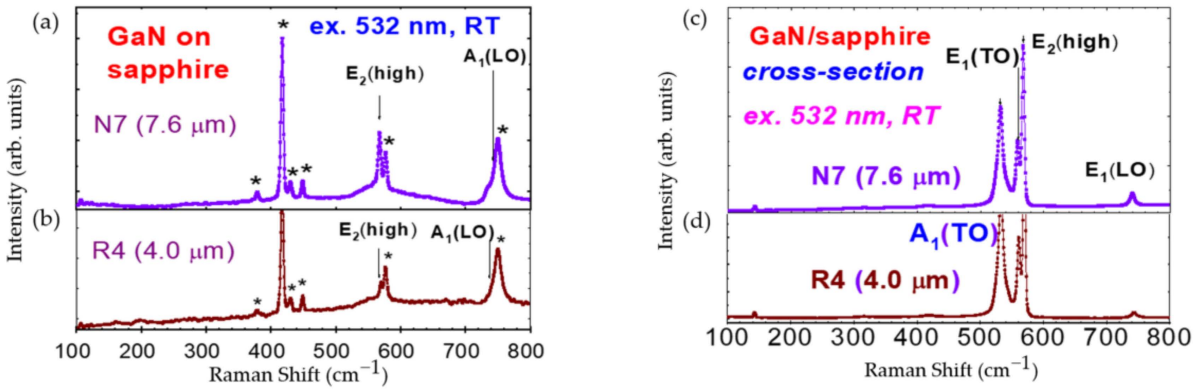


Figure 6. Raman spectra (ex. 532nm, RT) in normal backscattering configuration of GaN/sapphire (**a**) N7 and (**b**) R4, and at the GaN film cross-section (**c**) N7 and (**d**) R4, respectively. Marks * indicate Raman features from sapphire (Al_2O_3) crystal.

Figure 6c,d exhibit cross-section Raman spectra of these two GaN/sapphire samples, with the laser probe focusing on the GaN film region vertically, away from the sapphire substrate, and showing only Raman signals from crystalline GaN, without sapphire features and with GaN E_2(high) at ~568 cm^{-1} strongly. Two GaN A_1(TO) at 531 cm^{-1} and E_1(TO) at 559 cm^{-1} are observed to be relatively strong, which are forbidden along the c-plane GaN but allowed at the surface perpendicular to the c-axis of GaN [9,11].

Scanning Raman scattering measurements have been performed along the GaN film cross-section. Figure 7 shows that from the top spectral curve at the GaN surface, downwards to 8 μm away from the surface, and entering sapphire substrate area, the GaN peaks are weak and disappear afterwards. Both E_2(high) and E_1(LO) peak frequencies increase slightly from the GaN surface towards the GaN/sapphire interface.

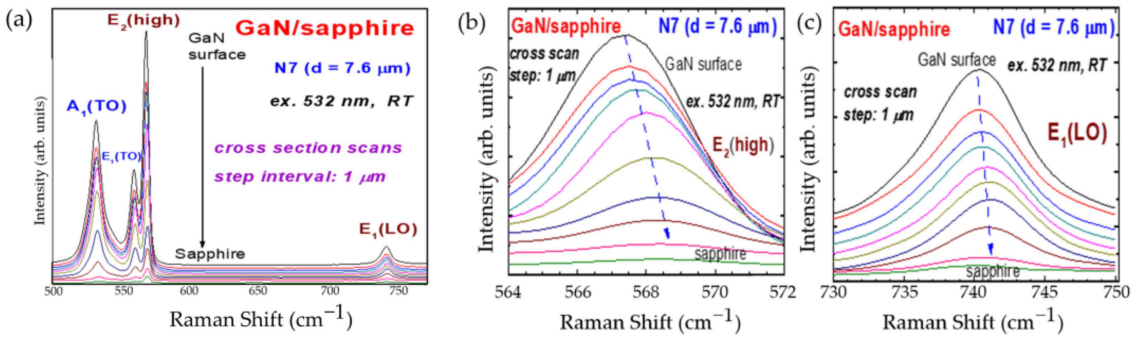


Figure 7. Scanning cross-section multiple Raman spectra (ex. 532 nm, RT) of GaN/sapphire N7 (d = 7.6 μm) with a step interval of 1 μm from the GaN surface into the sapphire substrate: (**a**) in 500–770 cm^{-1}, showing GaN phonon modes of A_1(TO) at ~531 cm^{-1}, E_1(TO) at ~559 cm^{-1}, E_2(high) at ~568 cm^{-1} and E_1(LO) at 741 cm^{-1}; (**b**) E_2(high) within 564–572 cm^{-1}, and (**c**) E_1(LO) within 730–750 cm^{-1}, respectively.

Figure 8 shows that the peak frequencies of these phonon modes again vary slightly along the GaN film cross-section between the GaN surface and the sapphire substrate. It shows that from the top spectra curve at the GaN surface, downwards to the 9th measurement, i.e., at 4.5 μm away from the surface, and entering the sapphire substrate area, the GaN peaks are weak and disappear after the 10th measurement. The trend is reversed in the case of the N7 (d = 7.6 μm) thick film: both E_2(high) and E_1(LO) peak frequencies decrease from the GaN surface towards the GaN/sapphire interface.

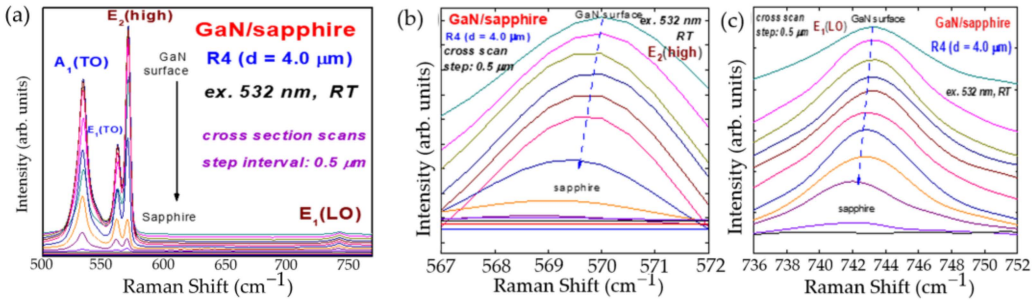


Figure 8. Scanning cross-section multiple Raman spectra (ex. 532 nm, RT) of GaN/sapphire sample R4 (d = 4.0 μm) with a step interval of 0.5 μm from GaN surface into sapphire substrate: (**a**) in Raman shift range of 500–770 cm^{-1}, showing GaN phonon modes of A_1(TO), E_1(TO), E_2(high) and E_1(LO); (**b**) E_2(high) spectral region of 567–572 cm^{-1}, and (**c**) E_1(LO) spectral area of 736–752 cm^{-1}, respectively.

The shift of the GaN E_2(high) phonon mode can be used to estimate the relative biaxial stress in heteroepitaxial GaN [8,14,35]. The Raman frequency difference $\Delta\omega$ relative to the stress-free E_2(high) frequency of 567.5 cm^{-1} was used to estimate the GaN layer stress σ using Equation (4).

$$\sigma = \Delta\omega / K \quad (4)$$

where K = 4.2 cm^{-1} GPa^{-1} is the conversion factor of GaN Raman biaxial stress. The E_2(high) peak positions in Figures 7b and 8b were obtained by Gaussian fitting and are listed in Tables 1 and 2 for samples N7 (7.6 μm) and R4 (4.0 μm), respectively.

Table 1. Gaussian-fitted E_2(high) peak frequencies and estimated stress for GaN/sapphire sample N7 (7.6 μm).

Distance (μm)	**0**	**1**	**2**	**3**	**4**	**5**	**6**	**7**	**8**	**9**
E_2 (high) χ (cm^{-1})	567.4	567.4	567.5	567.6	567.7	568.0	568.2	568.3	568.2	568.3
$\Delta\omega$ (cm^{-1})	−0.1	−0.1	0	0.1	0.2	0.5	0.7	0.8	0.7	0.8
Stress (GPa)	−0.024	−0.024	0	0.024	0.048	0.12	0.17	0.19	0.17	0.19

Table 2. Gaussian-fitted E_2(high) peak frequencies and estimated stress for GaN/sapphire sample R4 (4.0 μm).

Distance (μm)	**0**	**0.5**	**1.0**	**1.5**	**2.0**	**2.5**	**3.0**	**3.5**	**4.0**	**4.5**
E_2 (high) χ (cm^{-1})	570.2	570.1	569.9	569.8	569.6	569.6	569.6	569.5	569.3	569.25
$\Delta\omega$ (cm^{-1})	2.7	2.6	2.4	2.3	2.1	2.1	2.1	2.0	1.8	1.75
Stress (GPa)	0.64	0.62	0.57	0.55	0.50	0.50	0.50	0.48	0.43	0.42

The residual stress in GaN-on-sapphire may arise from both lattice mismatch during epitaxial growth and the difference in thermal expansion coefficients between GaN and sapphire during cooling. However, the present comparison does not isolate film thickness from other sample-specific growth conditions. Because only two samples are compared and their growth conditions were not independently controlled, the different stress profiles of N7 and R4 cannot be assigned solely to GaN layer thickness. The wurtzite GaN belongs to the hexagonal $P6_3mc$ space group with lattice constants of a_g = 0.3189 nm and c_g = 0.5185 nm, while the substrate sapphire (Al_2O_3) belongs to the trigonal $R\bar{3}c$ space group with a_s = 0.4578 nm and c_s = 1.2991 nm. There is also a difference between the thermal expansion coefficients of the two materials, 7.50 × 10^{-6} K^{-1} for sapphire and

5.45×10^{-6} K^{-1} for GaN. Lattice mismatch and thermal-expansion mismatch may both contribute to the residual biaxial stress in the GaN layer after cooling from the growth temperature. It has been pointed out that large biaxial stress may cause microcracks and degrade the optoelectronic properties of the epitaxial GaN layer [14,35].

Figures 7b and 8b, together with Tables 1 and 2, show different overall fitted E_2(high) peak-position profiles for N7 and R4. Because independent external verification and scan-specific repeatability data are unavailable, the individual point-to-point stress values are used only to describe the ranges calculated using Equation (4) rather than to identify quantitatively resolved local tensile-to-compressive transitions. For N7, the fitted E_2(high) peak positions range from 567.4 to 568.3 cm^{-1}, corresponding to calculated stress estimates from −0.024 to 0.19 GPa. For R4, the fitted peak positions range from 569.25 to 570.2 cm^{-1}, corresponding to stress estimates from 0.43 to 0.64 GPa. These ranges summarize the values calculated using Equation (4) and should not be interpreted as independently determined uncertainty intervals.

Figure 9 plots the fitted E_2(high) positions and corresponding stress estimates against nominal scan distance. Within the nominal GaN regions (0–7 μm for N7 and 0–4 μm for R4), the fitted peak position changes by approximately +0.90 cm^{-1} for N7 and −0.90 cm^{-1} for R4. This check does not include peak-fitting variability, signal-to-noise changes, focusing or spatial-averaging effects, or scan-to-scan repeatability. It therefore supports only the directions of the overall fitted profiles, not smaller point-to-point differences of approximately 0.05–0.30 cm^{-1} or apparent slope changes. The dashed lines are empirical guides. Because Ref. [13] examined laterally overgrown GaN/sapphire under different excitation and sampling conditions, its depth-dependent shifts are not directly comparable with the present data. Ref. [14] combined Raman measurements with HRXRD, whereas the present study lacks an independent structural measurement; therefore, the stress values reported here are treated as Raman-derived estimates.

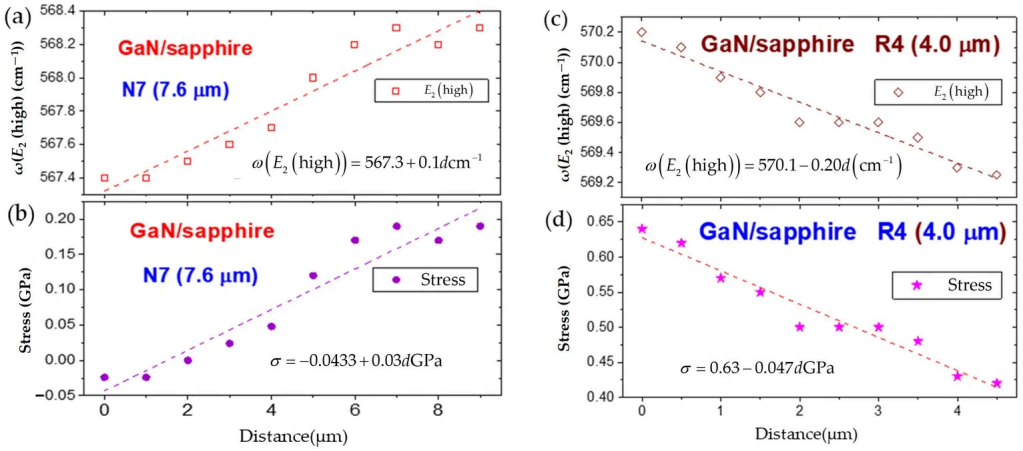


Figure 9. Fitted E_2(high) peak positions for (**a**) N7 and (**c**) R4 and the corresponding stress estimates for (**b**) N7 and (**d**) R4 as functions of the nominal scan distance. The dashed lines are empirical guides to the overall profiles.

3.4. Cross-Section Raman E_2(High) Mode SCM Fits

The spatial correlation model (SCM) was applied to the GaN E_2(high) mode using Equations (5) and (6) to obtain the effective phonon correlation length and intrinsic linewidth along the growth direction, as shown in Figures 10–12 and Tables 3 and 4 [8,9,36]. Conventional Hall measurements provide layer-averaged transport properties and do not directly resolve micrometer-scale variations along an exposed cross-section. Cross-sectional Raman spectroscopy provides spatially dependent, model-derived information that is complementary to Hall measurements.

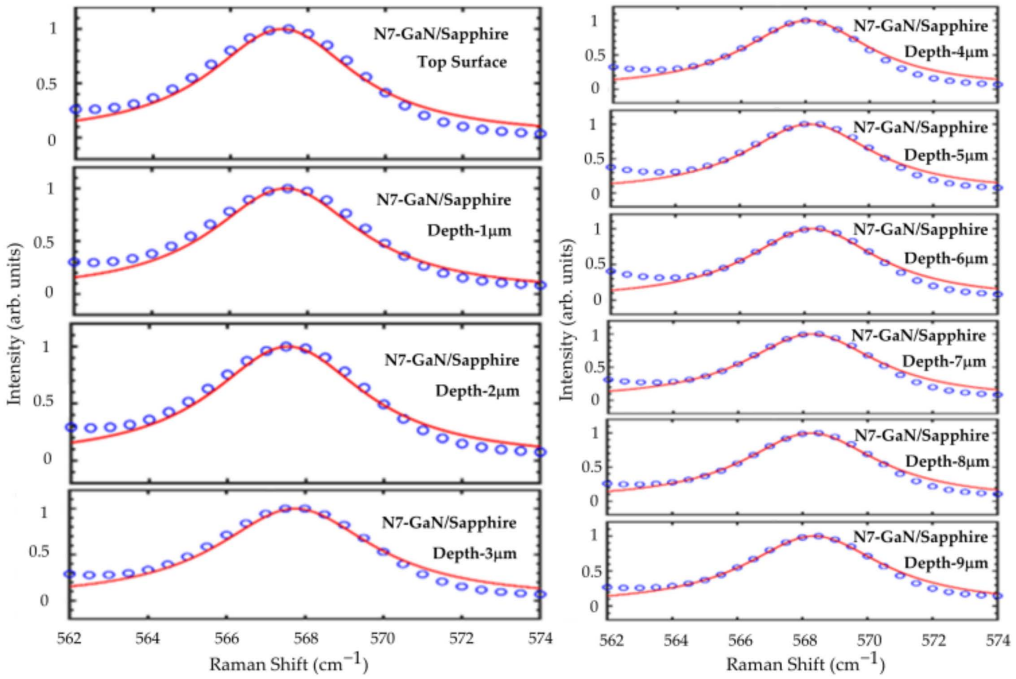


Figure 10. SCM fitting results for ten GaN E_2(high) spectra of GaN/sapphire sample N7 (7.6 μm). Experimental data are shown as blue open symbols, and fitted curves are shown as red lines.

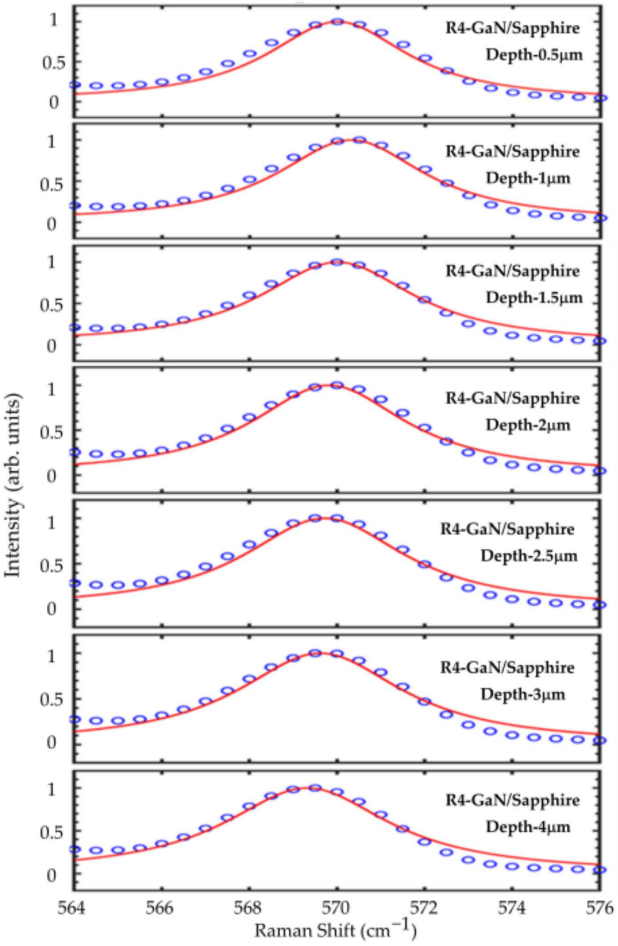


Figure 11. SCM model fitting results of seven GaN E_2(high) modes for GaN/sapphire R4 (4.0 μm) with experimental data in blue open symbols from Figure 8b and fitting results in red lines.

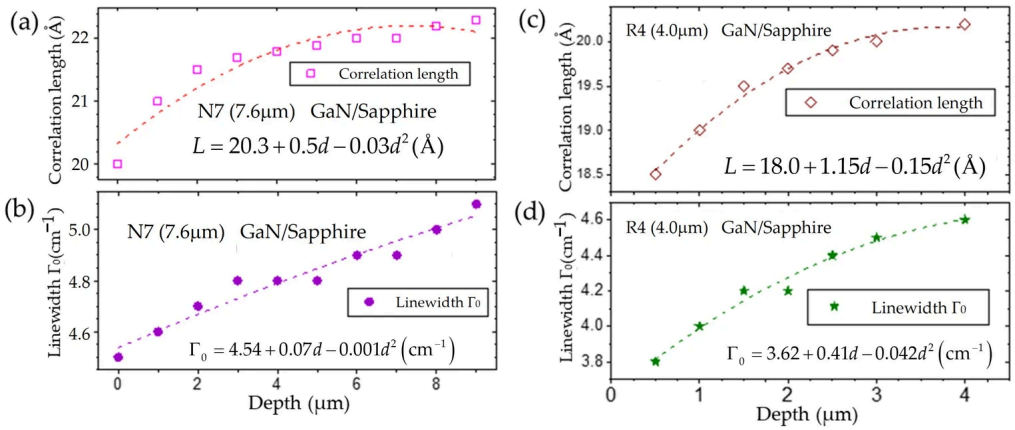


Figure 12. Depth d (μm) dependent spatial correlation model (SCM) fitted correlation length L (Å) and intrinsic line width Γ_0 (cm^{-1}) for GaN E_2 mode of two GaN/sapphire samples of N7 (7.6 μm) at (**a**,**b**) and R4 (4.0 μm) at (**c**,**d**), respectively. All correlation length L (Å) data values are shown with open symbols and line width Γ_0 (cm^{-1}) data values are shown with solid symbols.

Table 3. Spatial correlation model (SCM) fitted correlation length L (Å) and intrinsic line width Γ_0 (cm^{-1}) for the GaN E_2 mode of the GaN/sapphire sample N7 (7.6 μm).

Depth (μm)	0	1	2	3	4	5	6	7	8	9
E_2(high) ω(cm^{-1})	567.4	567.4	567.5	567.6	567.7	568.0	568.2	568.3	568.2	568.3
SCM fit A (cm^{-1})	567.3	567.5	567.6	567.8	568.1	568.2	568.3	568.3	568.3	568.4
SCM fit B (cm^{-1})	18	19	19.5	19.7	19.8	19.9	20	20.1	20.2	20.3
Correlation length L (Å)	20	21	21.5	21.7	21.8	21.9	22	22	22.2	22.3
SCM fit Γ_0 (cm^{-1})	4.5	4.6	4.7	4.8	4.8	4.8	4.9	4.9	5.0	5.1

Table 4. Spatial correlation model (SCM) fitted correlation length L (Å) and intrinsic line width Γ_0 (cm^{-1}) for the GaN E_2 mode of the GaN/sapphire sample R4 (4.0 μm).

Depth (μm)	0	0.5	1.0	1.5	2.0	2.5	3.0	3.5	4.0
E_2(high) ω(cm^{-1})	570	570.1	569.9	569.8	569.6	569.6	569.6	569.4	569.3
SCM fit A (cm^{-1})	570	570.0	570.3	570.0	569.8	569.7	569.6	569.4	569.3
SCM fit B (cm^{-1})	17	17.5	18.0	18.5	18.7	18.9	19.0	19.1	19.3
Correlation length L (Å)	18	18.5	19.0	19.5	19.7	19.9	20.0	20.2	20.2
SCM fit Γ_0 (cm^{-1})	3.6	3.8	4.0	4.2	4.2	4.4	4.5	4.5	4.6

Raman spectral intensity $I(\omega)$ of the GaN E_2(high) mode, by applying the spatial correlation model (SCM), can be described as [8,9]

$$I(\omega) \propto \int_0^1 exp\left(-q^2L^2/4\right) \frac{d^3q}{[\omega - \omega(q)]^2 + (\Gamma_0/2)^2} \quad (5)$$

where the reciprocal lattice q is in units of $2\pi/a$, a is the lattice constant, and Γ_0 is the natural or intrinsic linewidth. In the SCM, L represents an effective phonon correlation length associated with the spatial coherence of Raman-active phonons under translational-symmetry breaking. It is not equivalent to the average spacing of threading dislocations. The fitted values of 18.5–22.3 Å correspond to approximately 1.85–2.23 nm. The dispersion relation for optical phonon frequency $\omega(q)$ vs. the reciprocal lattice q has the form

$$\omega^2(q) = A + \left\{A^2 - B[1 - cos(\pi q)]\right\}^{1/2} \text{or } \omega(q) = A - Bq^2 \quad (6)$$

where A and B are adjustable parameters [8,9]. This spatial correlation model (SCM) has been used to study many semiconductors and oxides, including SiC, InGaN, InAlN, and GaN-AlN superlattices [8].

Figures 10 and 11 show the SCM fitting results for ten N7 spectra and seven R4 spectra, respectively. The experimental data are shown as blue open symbols, and the SCM fitting results are shown as red lines. Figure 10 presents the N7 spectra from d = 0 to 9 μm, whereas Figure 11 presents the R4 spectra from d = 0.5 to 4.0 μm. The fitted correlation length L (Å) and intrinsic linewidth Γ_0 (cm^{-1}) are listed in Tables 3 and 4.

According to the values listed in Tables 3 and 4, Figure 12 plots the graphs for depth d (μm) dependent spatial correlation model (SCM) fitted correlation length L (Å) and intrinsic line width Γ_0 (cm^{-1}) for the GaN E_2 mode of GaN/sapphire sample N7 (7.6 μm) at (a)–(b) and R4 (4.0 μm) at (c)–(d), respectively. Data values in each graph are fitted by polynomials up to the second order and expressed by dashed lines. The fitted polynomial expressions are given in each graph. The SCM fits yielded L values of 20.0–22.0 Å for N7 and 18.5–20.2 Å for R4, together with Γ_0 values of 4.5–5.1 cm^{-1} and 3.8–4.6 cm^{-1}, respectively. These ranges summarize the model-fitted values. Because repeatability and fit-parameter uncertainties are unavailable, the apparent point-to-point changes and polynomial curvature are not interpreted as quantitatively resolved depth trends.

In contrast to Ref. [12], which correlated spatially resolved Raman shifts with independently determined dislocation density, the present study has no independent defect-density measurement. Consequently, the fitted L values are reported only as effective phonon correlation lengths and are not converted into threading-dislocation spacing or density.

3.5. Cross-Sectional Raman E_1(LO)-Mode LOPC Fits

Raman LO mode is affected by free carriers and doping through LO–phonon–plasma coupling (LOPC). Theoretical studies describe the Raman LOPC mode intensity as [8,9,29,36]

$$I_{LOPC} = \left.\frac{d^2S}{d\omega d\Omega}\right|_A = \frac{16\pi h n_2}{V_0^2 n_1}\frac{\omega_2^4}{C^4}\left(\frac{d\alpha}{dE}\right)(n_\omega + 1)AIM\left(-\frac{1}{\varepsilon}\right) \quad (7)$$

where

$$A = 1 + 2C\frac{\omega_T^2}{\Delta}\left[\omega_p^2\gamma\left(\omega_T^2 - \omega^2\right) - \omega^2\eta\left(\omega^2 + \gamma^2 - \omega_p^2\right)\right] + C^2\left(\frac{\omega_T^4}{\Delta\left(\omega_L^2 - \omega_T^2\right)}\right) \times \left\{\omega_p^2\left[\gamma\left(\omega_L^2 - \omega_T^2\right) + \eta\left(\omega_p^2 - 2\omega^2\right)\right] + \omega^2\eta\left(\omega^2 + \gamma^2\right)\right\} \quad (8)$$

$$\Delta = \omega_p^2\gamma\left[\left(\omega_T^2 - \omega^2\right)^2 + (\omega\eta)^2\right] + \omega^2\eta\left(\omega_L^2 - \omega_T^2\right)\left(\omega^2 + \gamma^2\right) \quad (9)$$

In Equation (7), the parameters n_1 and n_2 represent the refractive indices at incident frequency ω_1 and scattered frequency ω_2, respectively. Constant C is the Faust–Henry coefficient of ~0.35, E the macroscopic electric field, α the material polarizability, and n_ω the Bose–Einstein population factor. For Equations (8) and (9), ω_p defines the plasma frequency, ω_L is the longitudinal optical (LO) phonon frequency, ω_T the transverse optical (TO) phonon frequency, η the phonon damping parameter, and γ the plasma oscillation damping.

Furthermore, the dielectric response ε can be expressed as

$$\varepsilon = \varepsilon_\infty\left(1 + \frac{\omega_L^2 - \omega_T^2}{\omega_T^2 - \omega^2 - i\omega\eta} - \frac{\omega_p^2}{\omega(\omega + i\gamma)}\right) \quad (10)$$

$$\omega_p^2 = \frac{4\pi N e^2}{\varepsilon_\infty m^*} \quad (11)$$

$$\gamma = e/(m^*\mu) \quad (12)$$

where ω_p is the plasma frequency, N the free carrier concentration, m^* the effective mass, e the elementary charge, and ε_∞ the high-frequency dielectric constant. Equations (7)–(12) have been applied for Raman analyses of GaN films [8,9,29,36]. Based on Equation (11), the carrier concentration is given by $N = \omega_p{}^2\ (\varepsilon_\infty\ m^*)/(4\pi e^2)$, while Equation (12) provides the mobility as $\mu = e/(m^*\ \gamma)$.

In polar semiconductors, LO phonons couple strongly to free-carrier plasmons. Using theoretical LOPC modeling, the GaN E_1(LO) modes in Figures 7c and 8c can be fitted [8,9,29,36] to extract carrier concentrations of GaN films on sapphire [8], Si [29] and 4H-SiC [36]. In the present work, this optical approach is employed to deduce the carrier concentration and mobility along the cross-section (growth direction) of GaN-on-sapphire films. Figures 13 and 14 compare the experimental E_1(LO) spectra with the LOPC-fitted curves for N7 and R4.

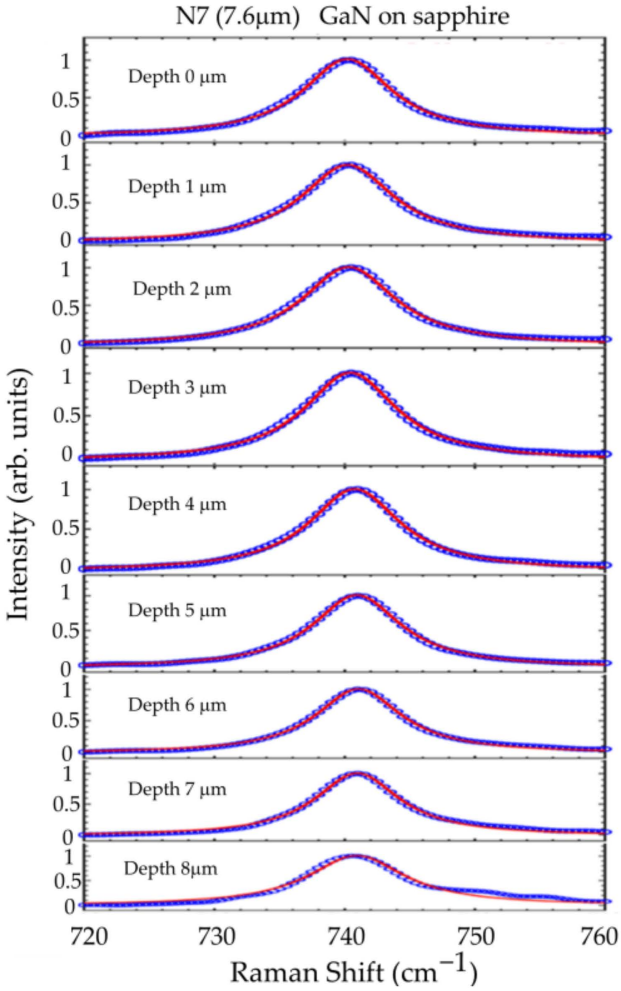


Figure 13. LOPC fits for GaN/sapphire N7 (7.6 μm), with the experimental data represented by blue open symbols from Figure 7c and the fitting results indicated by red lines according to Equations (7)–(12).

Tables 5 and 6 list the LOPC fitting parameters for N7 and R4, including carrier concentration N, mobility μ, plasma frequency ω_p, plasma damping rate γ_p, mean squared error (MSE), and root mean squared error (RMSE). MSE and RMSE characterize only the fitting residuals; they are not estimates of Raman-shift accuracy or parameter uncertainty.

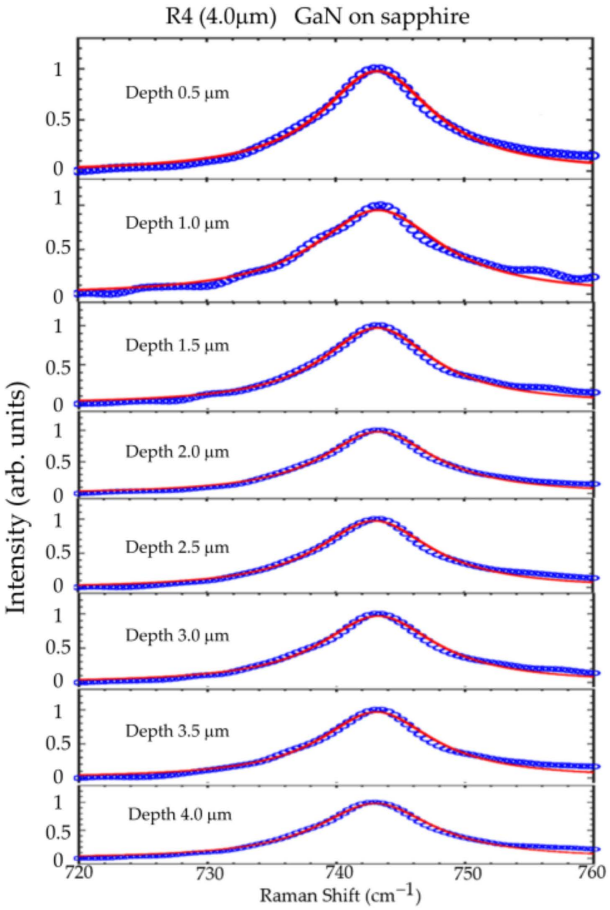


Figure 14. The LOPC fits for the GaN/sapphire sample R4 (4.0 μm), with experimental data represented by blue open symbols from Figure 8c and fitting results indicated by red lines according to Equations (7)–(12).

Table 5. Fitting parameters of GaN LOPC fit on RT Raman E_1(LO), N7 (n7600), d = 7.6 μm.

Depth (μm)	0 μm	1 μm	2 μm	3 μm	4 μm	5 μm	6 μm	7 μm	8 μm
E_1(LO) peak (cm^{-1})	740.2	740.2	740.3	740.4	740.8	740.9	741.1	741.0	740.9
E_1(LO) FWHM (cm^{-1})	8.36	8.70	8.77	8.69	8.49	8.25	8.02	7.91	9.06
ω_p (THz)	3.64	3.65	3.68	3.72	3.84	3.90	3.94	3.91	3.89
γ_p (THz)	0.25	0.26	0.26	0.26	0.25	0.25	0.24	0.24	0.27
N ($\times 10^{16}$ cm^{-3})	8.32	8.36	8.50	8.72	9.27	9.55	9.77	9.60	9.52
Mobility (cm^2/Vs)	1674	1608	1596	1611	1649	1696	1744	1769	1544
MSE (%)	0.02	0.03	0.02	0.02	0.02	0.01	0.02	0.05	0.28
RMSE (%)	1.62	1.87	1.54	1.49	1.52	1.08	1.61	2.27	5.29

Table 6. Fitting parameters of GaN LOPC fit on RT Raman E_1(LO), R4 (r4056), d = 4.0 μm.

Depth (μm)	0 μm	0.5 μm	1 μm	1.5 μm	2 μm	2.5 μm	3 μm	3.5 μm	4 μm
E_1(LO) peak (cm^{-1})	743.2	743.3	743.0	743.25	743.1	743.0	743.0	742.8	742.3
E_1(LO) FWHM (cm^{-1})	10.6	10.7	10.8	10.93	10.67	10.96	9.77	9.16	8.86
ω_p (THz)	4.62	4.65	4.58	4.64	4.60	4.57	4.56	4.52	4.35
γ_p (THz)	0.32	0.32	0.33	0.33	0.32	0.33	0.29	0.27	0.27
N ($\times 10^{17}$ cm^{-3})	1.34	1.36	1.32	1.36	1.33	1.32	1.31	1.28	1.19
Mobility (cm^2/Vs)	1325	1308	1291	1279	1311	1277	1433	1528	1580
MSE (%)	0.13	0.10	0.13	0.12	0.17	0.14	0.09	0.08	0.11
RMSE (%)	3.67	3.23	3.66	3.58	4.14	3.81	3.13	2.98	3.37

Based on the data values in Tables 5 and 6, Figure 15 shows depth d (μm) dependent LO phonon coupling (LOPC), model-fitted carrier concentration N (cm^{-3}) and electron mobility μ (cm^2/V s) for GaN E_1(LO) modes of GaN/sapphire N7 (7.6 μm) at (a) and R4 (4.0 μm) at (b), respectively. All carrier concentration N (cm^{-3}) data values are expressed in black symbols, and mobility μ (cm^2/V s) data values are in red symbols. Data values in each graph are fitted by polynomials up to the second order and expressed by dashed lines.

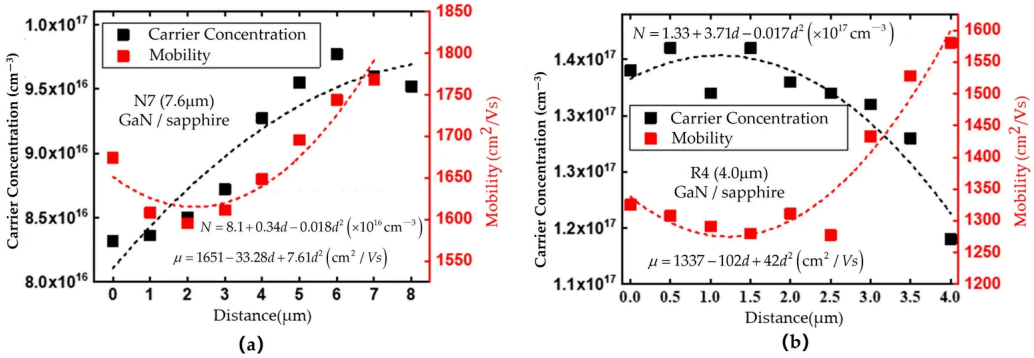


Figure 15. Depth d (μm) dependent LOPC model fits carrier concentration N (cm^{-3}) and electron mobility μ (cm^2/V s) for GaN E_1(LO) mode of GaN/sapphire (**a**) N7 (7.6 μm) and (**b**) R4 (4.0 μm), respectively.

Within the nominal GaN regions, the LOPC-derived carrier concentration ranges from 8.32×10^{16} to 9.77×10^{16} cm^{-3} for N7 and from 1.19×10^{17} to 1.36×10^{17} cm^{-3} for R4. The corresponding fitted mobility ranges are 1596–1769 $cm^2\ V^{-1}\ s^{-1}$ for N7 and 1277–1580 $cm^2\ V^{-1}\ s^{-1}$ for R4. Thus, N7 has a lower fitted carrier concentration and generally higher fitted mobility than R4.

The Raman–LOPC analysis indicates that the fitted carrier concentration and mobility do not exhibit a simple inverse relationship across the measured positions. In GaN/sapphire structures, carrier mobility may be affected not only by free-carrier concentration and plasmon damping but also by defect scattering, residual strain, dislocation-related disorder, and local crystal quality. Differences in defect distributions and unintentional impurity incorporation or compensation during epitaxial growth may contribute to the different carrier-parameter profiles of N7 and R4. However, because depth-resolved chemical-composition and independent defect-density measurements are unavailable, these mechanisms are considered possible explanations rather than direct experimental assignments. Taken together, Figures 9, 12 and 15 show different sample-specific fitted profiles of E_2(high)-derived relative stress, SCM-derived effective phonon correlation length, and LOPC-derived carrier parameters. N7 generally exhibits lower calculated compressive stress and higher fitted mobility than R4. Ref. [15] investigated a deliberately doped GaN device using a specified confocal configuration and independently evaluated spatial resolution. In contrast, the present LOPC-derived profiles are obtained from as-grown GaN layers without independently calibrated spatial resolution or Hall validation.

4. Conclusions

This study combines cross-sectional Raman measurements with model-based analyses of carrier concentration, electron mobility, stress, and crystalline properties in two MOCVD-grown GaN/sapphire samples. Two GaN-on-sapphire samples were characterized using cross-sectional scanning electron microscopy (SEM), optical transmission (OT), and spectroscopic ellipsometry (SE), providing complementary structural and optical information. The SE-derived apparent Urbach energies were 5.79 meV for N7 and 5.91 meV for R4.

Because these values are model-dependent, they are used only for comparison between the two samples and are not interpreted as direct measures of absolute defect density.

Raman spectra were acquired from the GaN surface toward the sapphire at nominal intervals of 1.0 μm for N7 and 0.5 μm for R4. The SENTERRA system calibrated each spectrum automatically and has a specified wavenumber-axis accuracy and precision better than 0.1 cm^{-1}. Within the nominal GaN regions, the fitted E_2(high) position changed by approximately +0.90 cm^{-1} for N7 and −0.90 cm^{-1} for R4. These signs are retained relative to the instrument specification, but smaller point-to-point shifts are not considered resolved because peak-fitting, focusing, spatial-averaging, and repeatability contributions are unavailable. SCM fits gave effective phonon correlation lengths of 20.0–22.3 Å for N7 and 18.5–20.2 Å for R4. LOPC fits gave carrier concentrations of 8.32×10^{16}–9.77×10^{16} cm^{-3} for N7 and 1.19×10^{17}–1.36×10^{17} cm^{-3} for R4, with mobility ranges of 1596–1769 and 1277–1580 $cm^2\ V^{-1}\ s^{-1}$, respectively. The SCM and LOPC quantities are model-dependent estimates rather than independently validated measurements.

Research and Development (R&D) on GaN-on-sapphire devices remains a priority for researchers. Key characteristics of GaN films, such as carrier concentration, electron mobility, layer stress and crystalline properties, along with their variations during film growth, are critical for advanced device fabrication. These results provide a sample-specific comparison of the depth-dependent Raman-derived properties of the two GaN/sapphire structures.

Author Contributions: Conceptualization, Z.C.F. and H.-L.L.; methodology, Z.C.F. and W.L.; software, K.Y. and J.Y.; validation, G.X., I.F. and C.C.; formal analysis, M.T.N., Y.-C.C. and K.Y.; investigation, S.B., M.T.N., Y.-C.C., Z.C.F., H.-L.L. and K.Y.; resources, H.-L.L., J.L., G.X., B.K. and I.F.; data curation, Y.-C.C.; writing—original draft preparation, G.C. and Z.C.F.; writing—review and editing, M.T.N., Z.C.F. and I.F.; visualization, J.Y., W.L. and C.C.; supervision, B.K. and I.F.; project administration, H.-L.L. and C.C.; funding acquisition, H.-L.L., J.L. and C.C. All authors have read and agreed to the published version of the manuscript.

Funding: This research was funded by the National Natural Science Foundation of China (Grant No. 51972319, 52305577).

Institutional Review Board Statement: Not applicable.

Informed Consent Statement: Not applicable.

Data Availability Statement: The data that support the findings of this study are available from the corresponding author, Z.C.F., upon reasonable request.

Acknowledgments: We acknowledge the help and support provided by Shiyuan Liu, Chuanwei Zhang and Lingyu Wan, in this work. H.L.L. thanks the Higher Education Sprout Project of National Taiwan Normal University. Z.C.F. acknowledges the support while working at National Taiwan University and Guangxi University.

Conflicts of Interest: Kang Yang and Jixiong Li were employed by the Wuhan Eoptics Technology Co., Ltd., Weijie Lu was employed by the Hexagonal Scientific Lab, LLC. The remaining authors declare that the research was conducted in the absence of any commercial or financial relationships that could be construed as a potential conflict of interest.

References

1. Melton, W.A.; Pankove, J.I. GaN growth on sapphire. *J. Cryst. Growth* **1997**, *178*, 168–173. [CrossRef]
2. Nakamura, S.; Pearton, S.; Fasol, G. *The Blue Laser Diode—The Complete Story*; Springer: Berlin, Germany, 2000. Available online: https://link.springer.com/book/10.1007/978-3-662-04156-7 (accessed on 2 May 2026).
3. Amano, H. Growth of GaN on sapphire via low-temperature deposited buffer layer and realization of p-type GaN by Mg doping followed by low-energy electron beam irradiation. *Rev. Mod. Phys.* **2015**, *87*, 1133–1138. (accessed on 3 May 2026). [CrossRef]
4. Gao, X.; Huang, Y.; Wang, R.; Sun, Y.; Wang, L. Advancing flexible optoelectronics with III-nitride semiconductors: From materials to applications. *Light Sci. Appl.* **2026**, *15*, 141. [CrossRef] [PubMed]

5. Di Paolo Emilio, M. (Ed.) *GaN Technology: Materials, Manufacturing, Devices and Design for Power Conversion*; Springer: Cham, Switzerland, 2024. [CrossRef]
6. Zhou, S.; Wan, Z.; Lei, Y.; Tang, B.; Tao, G.; Du, P.; Zhao, X. InGaN quantum well with gradually varying indium content for high-efficiency GaN-based green light-emitting diodes. *Opt. Lett.* **2022**, *47*, 1291–1294. [CrossRef] [PubMed]
7. Zhou, S.; Liao, Z.; Sun, K.; Zhang, Z.; Qian, Y.; Liu, P.; Du, P.; Jiang, J.; Lv, Z.; Qi, S. High-Power AlGaN-Based Ultrathin Tunneling Junction Deep Ultraviolet Light-Emitting Diodes. *Laser Photonics Rev.* **2024**, *18*, 2300464. [CrossRef]
8. Feng, Z.C. *Raman Scattering on Emerging Semiconductors and Oxides*; CRC Press: Boca Raton, FL, USA, 2024; ISBN 9781032638874. Available online: https://www.routledge.com/9781032638874 (accessed on 16 September 2026).
9. Feng, Z.C.; Wang, W.; Chua, S.J.; Zhang, P.; Williams, K.P.J.; Pitt, G.D. Raman scattering properties of GaN materials and structures under visible and ultraviolet excitations. *J. Raman Spectrosc.* **2001**, *32*, 840–846. [CrossRef]
10. Feng, Z.C.; Li, K.; Hou, Y.T.; Zhao, J.; Lu, W.; Collins, W.E. A comparative study of high-resolution transmission electron microscopy, atomic force microscopy and infrared spectroscopy for GaN thin films grown on sapphire by metalorganic chemical vapor deposition. *Surf. Coat. Technol.* **2006**, *200*, 3224–3229. [CrossRef]
11. Takeuchi, K.; Ogura, H.; Hasuike, N.; Kamikawa, T. Decomposition of the anisotropic strain in 3D-structure GaN layers using Raman spectroscopy. *Sci. Rep.* **2024**, *14*, 3330. [CrossRef] [PubMed]
12. Nootz, G.; Schulte, A.; Chernyak, L.; Osinsky, A.; Jasinski, J.; Benamara, M.; Liliental-Weber, Z. Correlations between spatially resolved Raman shifts and dislocation density in GaN films. *Appl. Phys. Lett.* **2002**, *80*, 1355–1357. [CrossRef]
13. Chaldyshev, V.V.; Pollak, F.H.; Pophristic, M.; Guo, S.P.; Ferguson, I. Micro-Raman investigation of thin lateral epitaxial overgrown GaN/sapphire(0001) films. *J. Appl. Phys.* **2002**, *92*, 6601–6606. [CrossRef]
14. Duan, H.; Gu, W.; Zhang, J.; Hao, Y.; Chen, C.; Ni, J.; Xu, S. Characterization of GaN grown on 4H-SiC and sapphire by Raman spectroscopy and high resolution XRD. *J. Semicond.* **2009**, *30*, 073001. [CrossRef]
15. Belyaev, A.E.; Strelchuk, V.V.; Nikolenko, A.S.; Romanyuk, A.S.; Mazur, Y.I.; Ware, M.E.; DeCuir, E.A., Jr.; Salamo, G.J. Depth profiling of strain and carrier concentration by cleaved surface scanning of GaN Gunn-diode: Confocal Raman microscopy. *Semicond. Sci. Technol.* **2013**, *28*, 105011. [CrossRef]
16. Hong, S.; Kim, S.; Kim, H.; Song, I.; Kim, J.H.; Kim, G. Optical characterization of GaN-based LED devices through spectroscopic ellipsometry. *Opt. Laser Technol.* **2025**, *184*, 112560. [CrossRef]
17. Suraj; Rathkanthiwar, S.; Raghavan, S.; Selvaraja, S.K. Polarization-independent grating in a GaN-on-sapphire photonic integrated circuit. *Opt. Express* **2023**, *31*, 23350–23361. [CrossRef] [PubMed]
18. Wang, J.B.; Li, X.D.; Chen, L.; Liu, T.; Han, Z.F.; You, S.H.; Wang, L.Z.; Li, Z.L.; Hao, Y.; Zhang, J.C. Report of GaN HEMTs on 8-in Sapphire. *IEEE Trans. Electron Devices* **2024**, *71*, 4429–4432. [CrossRef]
19. Li, S.; Zhang, H.W.; Ma, Y.F.; Wang, Q.H.; Ke, W.; Xia, Y.Y.; Wu, L.K.; Li, Y.H.; Zhu, T.G.; Ye, R.; et al. Investigation on the Isolation Approaches for High-Voltage GaN-on-Sapphire Monolithic Power Integrated Circuits. *Micromachines* **2025**, *16*, 1336. [CrossRef] [PubMed]
20. Kinstler, A.D.; Neumann, R.; Taylor, A.A.; Besendörfer, S.; Meissner, E.; Weingärtner, R.; Brunner, F.; Brusaterra, E.; Treidel, E.B.; Schulze, J. Direct investigation of localized leakage currents in GaN-on-sapphire pn-diode. *Sci. Rep.* **2025**, *15*, 39578. [CrossRef] [PubMed]
21. Paszkiewicz, B.K.; Paszkiewicz, B.; Dziedzic, A. Acoustic Emission from GaN-on-Sapphire Structures. *Electronics* **2025**, *14*, 4146. [CrossRef]
22. Jose, C.; Areeckal, A.S.; Francis, A.; Awadhiya, B. Graded barrier AlGaN/GaN MOS-HEMT for ultra-sensitive and label-free detection of SARS-CoV-2. *Micro Nanostruct.* **2026**, *209*, 208379. [CrossRef]
23. Kamiyama, M.; Rathkanthiwar, S.; Quiñones, C.E.; Mita, S.; Reddy, P.; Kirste, R.; Collazo, R.; Sitar, Z. Hole transport analysis in N-polar p-GaN. *J. Appl. Phys.* **2026**, *139*, 075706. [CrossRef]
24. Abdullah, N.H.; Abu Bakar, A.S.; Abdul Khudus, M.I.M.; Mustaffa, M.S.; Kamarundzaman, A.; Rizuan, N.; Zaidi, N.J. The trade-off between electrical performance and structural quality in silicon (n-type) and magnesium (p-type)-doped a-plane gallium nitride (GaN) on r-plane sapphire. *J. Mater. Sci. Mater. Electron.* **2026**, *37*, 989. [CrossRef]
25. Schmidtling, T.; Pohl, U.W.; Richter, W.; Peters, S. In situ spectroscopic ellipsometry study of GaN nucleation layer growth and annealing on sapphire in metal-organic vapor-phase epitaxy. *J. Appl. Phys.* **2005**, *98*, 033522. [CrossRef]
26. Charles, M.B.; Kappers, M.J.; Humphreys, C.J. The effect of AlGaN and SiN interlayers on GaN/Si(111). *Phys. Status Solidi C* **2005**, *2*, 956–959. [CrossRef]
27. Muth, J.F.; Lee, J.H.; Shmagin, I.K.; Kolbas, R.M.; Casey, H.C., Jr.; Keller, B.P.; Mishra, U.K.; DenBaars, S.P. Absorption coefficient, energy gap, exciton binding energy, and recombination lifetime of GaN obtained from transmission measurements. *Appl. Phys. Lett.* **1997**, *71*, 2572–2574. [CrossRef]
28. Liu, W.-S.; Chang, Y.-L.; Tan, C.-Y.; Tsai, C.-T.; Kuo, H.-C. Properties of N-Type GaN Thin Film with Si-Ti Codoping on a Glass Substrate. *Crystals* **2020**, *10*, 582. [CrossRef]

29. Feng, Z.C.; Liu, J.M.; Xie, D.; Nafisa, M.T.; Zhang, C.W.; Wan, L.Y.; Jiang, B.B.; Lin, H.H.; Qiu, Z.R.; Lu, W.J.; et al. Optical, structural and synchrotron X-ray absorption studies for GaN thin films grown on Si by molecular beam epitaxy. *Materials* **2024**, *17*, 2921. [CrossRef] [PubMed]
30. Piccardo, M.; Li, C.K.; Wu, Y.R.; Speck, J.S.; Bonef, B.; Farrell, R.M.; Filoche, M.; Martinelli, L.; Peretti, J.; Weisbuch, C. Localization landscape theory of disorder in semiconductors. II. Urbach tails of disordered quantum well layers. *Phys. Rev. B* **2017**, *95*, 144205. [CrossRef]
31. Chichibu, S.; Mizutani, T.; Shioda, T.; Nakanishi, H.; Deguchi, T.; Azuhata, T.; Sota, T.; Nakamura, S. Urbach–Martienssen tails in a wurtzite GaN epilayer. *Appl. Phys. Lett.* **1997**, *70*, 3440–3442. [CrossRef]
32. Finn, R.; O'Donovan, M.; Koprucki, T.; Schulz, S. Impact of carrier-density screening on Urbach-tail energies and optical polarization in (Al,Ga)N quantum well systems. *Phys. Rev. Appl.* **2025**, *24*, 044084. [CrossRef]
33. Ugur, E.; Ledinsky, M.; Allen, T.G.; Holovsky, J.; Vlk, A.; De Wolf, S. Life on the Urbach Edge. *J. Phys. Chem. Lett.* **2022**, *13*, 7702–7711. [CrossRef] [PubMed]
34. Ledinsky, M.; Schönfeldova, T.; Holovsky, J.; Aydin, E.; Hajkova, Z.K.; Landova, L.; Neykova, N.; Fejfar, A.; De Wolf, S. Temperature Dependence of the Urbach Energy in Lead Iodide Perovskites. *J. Phys. Chem. Lett.* **2019**, *10*, 1368–1373. [CrossRef] [PubMed]
35. Margueron, S.H.; Bourson, P.; Gautier, S.; Soltani, A.; Troadec, D.; De Jaeger, J.-C.; Sirenko, A.A.; Ougazzaden, A. Residual stress relaxation in GaN/sapphire circular pillars measured by Raman scattering spectroscopy. *J. Cryst. Growth* **2008**, *310*, 5321–5326. [CrossRef]
36. Cui, C.C.; Nafisa, M.T.; Feng, Z.C.; Xu, G.; Yiin, J.; Liu, Y.; Lu, W.J.; Klein, B.; Ferguson, I.T. Spectroscopic ellipsometry and correlated studies of GaN films on 4H-SiC by MOCVD. *Vacuum* **2025**, *240*, 114589. [CrossRef]

Disclaimer/Publisher's Note: The statements, opinions and data contained in all publications are solely those of the individual author(s) and contributor(s) and not of MDPI and/or the editor(s). MDPI and/or the editor(s) disclaim responsibility for any injury to people or property resulting from any ideas, methods, instructions or products referred to in the content.